POLITECNICO DI TORINO
Repository ISTITUZIONALE

Transfer fields and Langevin forces for the noise analysis in diffusive nanodevices within the nonequilibrium Green's function approach

Original
Transfer fields and Langevin forces for the noise analysis in diffusive nanodevices within the nonequilibrium Green's function approach / Bertazzi, F., Tibaldi, A., Gonzalez Montoya, J.A., Mercinelli, F., Goano, M., Donati Guerrieri, S., Bonani, F., Ghione, G.. - In: PHYSICAL REVIEW APPLIED. - ISSN 2331-7019. - STAMPA. - 24:3(2025), pp. 1-13. [10.1103/q7h9-y56h]

Availability:
This version is available at: 11583/3002840 since: 2025-12-01T06:53:10Z

Publisher:
APS

Published
DOI:10.1103/q7h9-y56h

Terms of use:

This article is made available under terms and conditions as specified in the corresponding bibliographic description in the repository

Publisher copyright
APS postprint/Author's Accepted Manuscript e postprint versione editoriale/Version of Record

This article appeared in PHYSICAL REVIEW APPLIED, 2025, 24, 3, and may be found at ttp://dx.doi.org/10.1103/q7h9-y56h. Copyright 2025 American Physical Society

(Article begins on next page)

18 November 2026

Transfer fields and Langevin forces for the noise analysis in diffusive nanodevices within the nonequilibrium Green's function approach

Francesco Bertazzi[(1,2)],* Alberto Tibaldi[(1)],† Jesus Alberto Gonzalez Montoya[(1)], Francesco Mercinelli[(1)], Michele Goano[(1,2)], Simona Donati Guerrieri[(1)], Fabrizio Bonani[(1)], and Giovanni Ghione[(1)]
(1) DET, Politecnico di Torino, Torino, Italy and
(2) IEIIT-CNR, Torino, Italy
(Dated: September 18, 2025)

Advanced applications based on semiconductor nanostructures require accurate modeling tools for the description of coherent and dissipative quantum processes, but, crucially, also microscopic fluctuations and their propagation to the contacts. Being the two aspects, conduction and fluctuations, intimately related by the fluctuation-dissipation theorem, the analysis of carrier transport and noise properties should be addressed at the same level of approximation to obtain a complete and unambiguous understanding of the quantum system. Starting from a quantum transport model based on the nonequilibrium Green's function formalism, we identify a set of microscopic noise sources in terms of fundamental current and charge fluctuations in the presence of dissipative processes. The noise sources are added to the relevant conservation equations, and the power spectra of the short-circuit current fluctuations are evaluated through a linear perturbation theory equivalent to the classical impedance field method for noise analysis. Numerical examples with textbook structures are shown to establish a connection with semiclassical noise theories. Application to a resonant tunneling diode shows the potential of the proposed model as a tool to probe the electron kinetics in highly nanostructured devices. The present work concerns fluctuations associated with intraband scattering processes. The extension to number fluctuations due to interband scattering could provide information on the technological quality and physical origin of degradation mechanisms in state-of-the-art optoelectronic devices such as type-II superlattice photodetectors.

I. INTRODUCTION

A unified description of carrier transport and noise properties beyond semiclassical approximations is needed to assess the potential of advanced optoelectronic applications based on highly nanostructured materials. Probing fluctuations in nanostructures may provide valuable information on carrier transport properties that would not be directly accessible to (average) DC steady-state characterizations [1]. For example, carrier mobilities are intimately related to noise, and in fact "noise diffusivity" in bulk materials is usually evaluated from the autocorrelation function of velocity fluctuations in Monte Carlo simulations [2]. The Fano factor, the ratio of the shot noise power to its full Poissonian value, is highly indicative of the nature of carrier transport. Deviations from the shot noise behavior have been studied in resonant tunneling diodes [3, 4] and superlattices [5–7], revealing the relative importance of coherent propagation, and dissipative, phase-breaking processes in different bias conditions. Correlations between $1/f$ noise and specific dark current components (shunt, generation–recombination, and trap-assisted tunneling currents) have been observed in type-II superlattice (T2SL) infrared detectors [8]. Finally, low-frequency noise characterization is also a sensitive tool to investigate device quality, reliability, and the physical origin of degradation mechanisms [9, 10].

Physics-based noise analysis in semiconductor devices is usually carried out in the drift-diffusion (DD) approximation, assuming small fluctuations and converting the linearized physical model into a Langevin equation, i.e., a partial differential equation complemented with stochastic forcing terms, the Langevin forces [11, 12]. The drift-diffusion model is just the starting point of a hierarchy of hydrodynamic transport models [13], which can be formally derived, including microscopic noise sources, from the statistical moments of the Langevin–Boltzmann equation (LBTE), the fundamental equation for particle transport and noise in semiclassical physics [14, 15]. Besides moment-based methods derived from the LBTE, Monte Carlo simulations have been extensively used to evaluate velocity and population fluctuations in bulk materials and devices by solving directly for the BTE [2, 16, 17]. By mimicking the physics of scattering, the method directly provides microscopic variables as realization of random processes, thus allowing to separate fluctuations from averages [18]. However, the common semiclassical origin of these models makes them unsuitable for the analysis of noise in highly nanostructured devices [19].

Among genuine quantum approaches, the nonequilibrium Green's function (NEGF) formalism is the most versatile and powerful. With foundations in advanced concepts of many-body and quantum field theories, NEGF has found wide-spread application in the modeling of advanced (opto)electronic nanodevices [20–22]. Being noise essentially a two-particle property [23], [24, Ch. 13], conventional expressions in terms of single-particle Green's functions obtained from Wick's theorem are formally exact only in the noninteracting limit [3, 25–28], in which

* francesco.bertazzi@polito.it
† alberto.tibaldi@polito.it

the Landauer-Büttiker noise formula based on the scattering matrix formalism [29] is recovered. In the presence of scattering processes breaking the coherent propagation of the carriers, additional vertex corrections should be added to the mean-field contribution of noise. Although scattering processes are somehow included in mean-field expressions if Green's functions and self-energies are computed self-consistently, omitting these vertex corrections would lead, even in the limit of weak interaction, to a violation of the fluctuation-dissipation theorem [30]. A very elegant formalism to overcome the limitations of mean-field theories, is the full counting statistics, a theory originally introduced in the 90's by Levitov and Lesovik, motivated by studies on photon counting [31]. An extension of the standard NEGF scheme incorporating counting fields allows to address current correlations and higher-order current cumulants, while taking consistently into account all contributions due to electron-phonon coupling up to a given order in perturbation theory [30, 32].

Recently, we proposed an accurate, yet computationally efficient nonequilibrium Green's function model of dissipative carrier transport to study DC and AC small-signal properties of semiconductor nanostructures [33, 34]. As the model features a strong connection with conventional drift-diffusion solvers, it is tempting to formulate the problem of noise along the same lines of the drift-diffusion approach [11, 35], i.e., to treat the fluctuations generated by microscopic noise sources within the device as small perturbations within respect to a steady-state solution, and then propagate these fluctuations to the contacts by means of the transfer function obtained from the linearized model (a similar approach was reported in [36]). Being the linearized model already available from the small-signal analysis [34], the remaining task is the calculation of the microscopic sources, i.e., the Langevin forces.

The crucial approximation that enables the numerical evaluation of the Green's functions and their functional derivatives needed in the small-signal model – a local, Büttiker-probe description of carrier-phonon scattering within the self-consistent Born approximation – is also the key to define the microscopic noise sources: the Büttiker probes can be simply regarded as additional terminals, whose charge and current fluctuations can be computed with the multi-terminal scattering matrix theory developed in [29]. The resulting microscopic noise sources are spatially correlated and colored, as opposed to the uncorrelated and white sources usually adopted in Langevin-based approaches based on the DD approximation. Moreover, the NEGF model accounts also for charge fluctuations and more in general for long-range Coulomb correlations [17, 37], when the electric field profile is solved self-consistently.

II. THEORY

A very general form of the conservation equations valid for both NEGF and drift-diffusion models reads for one-dimensional nanostructures

$$\frac{\partial}{\partial z}\left(\epsilon\frac{\partial}{\partial z}\phi\right) = -\mathrm{e}\,(p - n + N_{\mathrm{D}}) \tag{1a}$$

$$\frac{\partial n}{\partial t} = +\frac{1}{\mathrm{e}}\frac{\partial J_n}{\partial z} - U_n \tag{1b}$$

$$\frac{\partial p}{\partial t} = -\frac{1}{\mathrm{e}}\frac{\partial J_p}{\partial z} - U_p, \tag{1c}$$

where ϵ is the background dielectric constant, N_{D} is the net donor impurity concentration, n and p are the carrier concentrations within the nanostructure, $J_{n,p}$ the electron and hole current densities, and $U_{n,p}$ the net electron and hole recombination rates, whose expressions depends on the generation-recombination mechanisms included in the simulation. Before we proceed with the linearization procedure, it is convenient to include two additional equations to define the circuit-oriented noise parameters. Assuming that the device is voltage driven [38] and choosing the left contact as the active one, we complement the equations above with the circuit equation

$$V_{\mathrm{L}} = V_{\mathrm{bias}}, \tag{1d}$$

and the current equation (including both particle and displacement components)

$$I_{\mathrm{L}} = \mathcal{A}\left[J_n + J_p + \epsilon\frac{\partial}{\partial t}\frac{\partial\phi}{\partial z}\right]_{z=z_{\mathrm{L}}}, \tag{1e}$$

where $\mathcal{A}$ is the device cross-sectional area. Analogous equations for the right contact have been introduced in our numerical implementation to verify the conservation of noise spectra, but are not included here for the sake of brevity. The inclusion of (1d) in the model equations may appear redundant for a nanostructure driven by ideal voltage sources. The constitutive relations of the embedding circuit are strictly needed only in mixed-mode simulations, but, as will be discussed in the following, the inclusion of the additional variable V_{L} simplifies the calculation of the small-signal admittance needed for the evaluation of the Nyquist noise limit.

Assuming as unknowns the electrostatic potential ϕ, the electron and hole quasi-Fermi levels μ_n, μ_p (the Fermi levels of the Büttiker probes in the NEGF formulation), the voltage drop V_{L} across the device, and the current I_{L}, the model equations (1) can be compactly written as

$$F_\alpha(\phi, \mu_n, \mu_p, V_{\mathrm{L}}, I_{\mathrm{L}}) = 0, \tag{2}$$

where $\alpha = \phi, \mu_n, \mu_p, V_{\mathrm{L}}, I_{\mathrm{L}}$ labels the equations from (1a) to (1e). In order to perform the noise analysis, a small-amplitude stochastic forcing term, the Langevin force $\xi_\alpha(z,t)$, is added to the right-hand side of (2), thus perturbing the DC noiseless operating point

$(\phi_0, \mu_{n0}, \mu_{p0}, V_{\mathrm{L}0}, I_{\mathrm{L}0})$, and resulting in the Langevin equation

$$F_\alpha(\phi_0+\delta\phi, \mu_{n0}+\delta\mu_n, \mu_{p0}+\delta\mu_p, V_0+\delta V_\mathrm{L}, I_{\mathrm{L}0}+\delta I_\mathrm{L}) + \frac{\partial \delta n}{\partial t}\delta_{\alpha\mu_n} + \frac{\partial \delta p}{\partial t}\delta_{\alpha\mu_p} + \epsilon \frac{\partial}{\partial t}\frac{\partial \delta\phi}{\partial z}\bigg|_{z_\mathrm{L}} \delta_{\alpha I_\mathrm{L}} = \xi_\alpha. \tag{3}$$

Under the condition of small-amplitude time-varying perturbation of the source term, the device equations can be linearized around the DC working point, thus yielding the small-signal system in the frequency domain:

$$\Lambda_\alpha(\delta\phi, \delta\mu_n, \delta\mu_p, \delta V_\mathrm{L}, \delta I_\mathrm{L}) + D_\alpha(\delta\phi, \delta\mu_n, \delta\mu_p, \omega) = \xi_\alpha(\omega), \tag{4}$$

where the linearized functionals Λ_α and D_α are defined as

$$\Lambda_\alpha(\delta\phi, \delta\mu_n, \delta\mu_p, \delta V_\mathrm{L}, \delta I_\mathrm{L}) = \frac{\partial F_\alpha}{\partial \phi}\delta\phi + \frac{\partial F_\alpha}{\partial \mu_n}\delta\mu_n + \frac{\partial F_\alpha}{\partial \mu_p}\delta\mu_p + \frac{\partial F_\alpha}{\partial V_\mathrm{L}}\delta V_\mathrm{L} + \frac{\partial F_\alpha}{\partial I_\mathrm{L}}\delta I_\mathrm{L} \tag{5a}$$

$$D_\alpha(\delta\phi, \delta\mu_n, \delta\mu_p, \omega) = \mathrm{i}\omega\left[\left(\frac{\partial \delta n}{\partial \phi}\delta\phi + \frac{\partial \delta n}{\partial \mu_n}\delta\mu_n\right)\delta_{\alpha\mu_n} + \left(\frac{\partial \delta p}{\partial \phi}\delta\phi + \frac{\partial \delta p}{\partial \mu_p}\delta\mu_p\right)\delta_{\alpha\mu_p} + \frac{\partial I_{Ld}}{\partial \phi}\delta_{\alpha I_\mathrm{L}}\right], \tag{5b}$$

where I_{Ld} is the displacement current at the left contact, and all derivatives are evaluated at the steady-state solution. In order to compute the short-circuit current fluctuation spectra, let us define the transfer field $\mathcal{G}_{I\beta}$ as the small-signal response of the terminal current to an impulsive source term $\delta_{I\beta}\,\delta(z-z')$ added to right-hand side of the linearized current equation. Then, the fluctuation of the terminal current induced by the microscopic noise source ξ_β is given by

$$\delta I_\mathrm{L}(\omega) = \sum_\beta \int \mathrm{d}z\, \mathcal{G}_{I\beta}(z,\omega)\xi_\beta(z,\omega), \tag{6}$$

with $\beta = \phi, \mu_n, \mu_p, V_\mathrm{L}, I_\mathrm{L}$. Application of the Wiener-Lee theorem delivers the desired power spectrum of the current fluctuations

$$S_{II}(\omega) = \sum_{\gamma,\delta}\iint \mathrm{d}z_1\mathrm{d}z_2 \mathcal{G}_{I\gamma}(z_1,\omega)K_{\xi_\gamma\xi_\delta}(z_1,z_2,\omega)\mathcal{G}^*_{\delta I}(z_2,\omega), \tag{7}$$

where $K_{\xi_\gamma\xi_\delta}(z_1,z_2,\omega)$ are the correlation spectra of the microscopic noise sources to be defined later.

The discussion so far was intentionally very general to emphasize the common framework of DD and NEGF noise models based on the impedance field method. In order to proceed further, we need to express the relevant quantities in terms of nonequilibrium Green's functions. For brevity, from this point forward, we report only the equations for electrons in the conduction band. A finite-difference discretization [39] of the steady-state Dyson and Keldysh equations gives the matrix equations (we assume a uniform mesh with spacing Δ [40])

$$G^R(E) = \left[E\mathbf{1} - H - \Sigma^R(E)\right]^{-1} \tag{8a}$$

$$G^<(E) = G^R(E)\Sigma^<(E)G^A(E), \tag{8b}$$

where $G^A = (G^R)^\dagger$, $\mathbf{1}$ is the identity matrix, and H is the (tridiagonal) Hamiltonian matrix (i is the nodal index)

$$\begin{cases} H_{ii} &= \hbar^2/(m_n^*\Delta^2) - \mathrm{e}\phi_i + \Delta E_{\mathrm{C},i} \\ H_{ii\pm1} &= -\hbar^2/(2m_n^*\Delta^2), \end{cases} \tag{9}$$

m_n^* is the electron effective mass, Δ is the mesh spacing, and ΔE_C is the conduction-band discontinuity (nonzero only for heterostructures). The retarded self-energy Σ^R includes boundary components to describe the coupling with the contacts, as well scattering components to model phase-breaking processes. Originally introduced to provide a simplified, phenomenological description of scattering, the Büttiker-probe formalism was recently extended to provide a more rigorous treatment of electron-phonon scattering within the self-consistent Born approximation [41]. We follow this approach to compute the self-energy Σ^R_{BP} due to deformation potential scattering mediated by acoustic and optical phonons, as described in [34].

To avoid nonphysical reflections at the boundaries [42], we include scattering also in the contacts. Extending the scattering self-energy Σ^R_{11} associated to the first Büttiker probe to the left contact, the recursive relation for the calculation of the corresponding boundary self-energy gives ($h = E\mathbf{1} - H$) [43]

$$\Sigma^R_\mathrm{L}(E) = \frac{h_{11} - \Sigma^R_{11} \pm \sqrt{\left(h_{11}-\Sigma^R_{11}\right)^2 - 4h_{12}^2}}{2}. \tag{10}$$

A similar expression holds for the boundary self-energy Σ^R_R of the right contact. The choice of the solution is determined by the requirement $\mathbb{I}\mathrm{m}\left\{\Sigma^R_{\mathrm{L,R}}\right\} < 0$ for a causal Green's function.

One of the advantages of the Büttiker-probe formalism is that the retarded components of the self-energies can be computed from the retarded Green's functions alone, while the lesser components are obtained from a fluctuation-dissipation relation, thus decoupling the calculation of retarded and lesser components. Since the Büttiker probes may be considered as additional contacts with Fermi levels μ_n, their self-energies being local in space as those describing the coupling to the contacts, we can use a unified notation for both physical and scattering contacts to write the diagonal entries of $\Sigma^<$ as

$$\Sigma^<_\alpha(E) = \mathrm{i}\mathcal{F}_\alpha(E)\Gamma_\alpha(E), \tag{11}$$

where $\Gamma_\alpha = \mathrm{i}\left(\Sigma^R_\alpha - \Sigma^A_\alpha\right)$ is the broadening function and $\mathcal{F}_\alpha(E)$ is the occupation factor computed as the integral over the transverse energy E_k of the Fermi-Dirac function $f_\alpha(E) = f_{\mathrm{FD}}(E-\mu_\alpha)$, multiplied by the two-dimensional density of states $N_{\mathrm{2D}} = 2_s m^*_n/(2\pi\hbar^2)$ (2_s being the spin factor)

$$\mathcal{F}_\alpha(E) = N_{\mathrm{2D}} \int \mathrm{d}E_k \, f_\alpha(E+E_k), \tag{12}$$

the index α running over the physical terminals of the device, i.e., the left and right contacts ($\alpha = L, R$), and the scattering terminals ($\alpha = 1 \cdots N$), i.e., the Büttiker probes.

With the definitions above, the finite-difference version of (2) is ($i = 1 \cdots N$ is a nodal index)

$$\sum_j P_{ij}\phi_j + \frac{\mathrm{i}}{\Delta}\int \frac{\mathrm{d}E}{2\pi} G^<_{ii}(E) - N_{\mathrm{D},i} = \xi^{(i)}_\phi \tag{13a}$$

$$\frac{1}{\Delta}\int \frac{\mathrm{d}E}{2\pi\hbar} 2\mathbb{R}e\{G^R(E)\Sigma^<_{\mathrm{BP}}(E) - G^<(E)\Sigma^A_{\mathrm{BP}}(E)\}_{ii} + \mathrm{i}\omega\frac{-\mathrm{i}}{\Delta}\int\frac{\mathrm{d}E}{2\pi}G^<_{ii}(E) - U_{n,i} = \xi^{(i)}_{\mu_n} \tag{13b}$$

$$V_{\mathrm{L}} - V_{\mathrm{bias}} = \xi_{V_{\mathrm{L}}} \tag{13c}$$

$$I_{\mathrm{L}} - \mathrm{e}\int \frac{\mathrm{d}E}{2\pi\hbar} 2\mathbb{R}e\{G^R_{11}(E)\Sigma^<_{\mathrm{L}}(E) - G^<_{11}(E)\Sigma^A_{\mathrm{L}}(E)\} - \mathrm{i}\omega\epsilon_1\frac{\phi_1-\phi_0}{\Delta} = \xi_{I_{\mathrm{L}}}, \tag{13d}$$

where P is the tridiagonal stiffness matrix arising from the finite-difference discretization of Poisson's equation

$$\begin{cases} P_{ii} &= (\varepsilon_{\mathrm{i}-1} + 2\varepsilon_{\mathrm{i}} + \varepsilon_{\mathrm{i}+1})/(\mathrm{e}\Delta^2) \\ P_{ii\pm1} &= -(\varepsilon_{\mathrm{i}} + \varepsilon_{\mathrm{i}\pm1})/(\mathrm{e}\Delta^2). \end{cases} \tag{14}$$

Notice that the self-energies appearing in (13b) include only the scattering component associated to the Büttiker probes. At equilibrium, we set $\mu_n = 0$, and we are left only with the Poisson's equation (13a), which is solved with floating boundary conditions for ϕ^{eq} [34]. Out of equilibrium, the full set of equations is first solved in steady-state conditions by means of a Newton algorithm to find the noiseless working point. Then, an augmented version of the small-signal model presented in [34] is solved for the transfer fields. The sum over the index j in (13a) is extended from 0 to $N+1$ to shift the Dirichlet boundary conditions one mesh step away from the boundaries on either side of the nanostructure

$$\phi_0 = \phi^{\mathrm{eq}}_1 + V_{\mathrm{L}} \tag{15a}$$

$$\phi_{N+1} = \phi^{\mathrm{eq}}_N, \tag{15b}$$

so that the transfer fields will be defined over the whole simulation domain, including also the first and last node. The current conserving boundary conditions introduced in [34] for the continuity equation (13b) are modified accordingly: the Fermi levels of the contacts are now fixed by the applied bias V

$$\mu_{\mathrm{L}} = -\mathrm{e}V_{\mathrm{L}} \tag{16a}$$

$$\mu_{\mathrm{R}} = 0, \tag{16b}$$

while the Büttiker-probe Fermi levels at the contacts are considered as variables to accommodate current conservation. The net recombination rate U_n describing, e.g., radiative and SRH transitions, may be computed using semiclassical expressions in terms of carrier densities [33], or from appropriate interband scattering self-energies if a multiband model of the electronic structure is employed [44]. Since the focus of this work is on noise due to intraband scattering processes, we will not discuss U_n further. We will postpone the study of population fluctuations to a future work.

Separating the system variables into two sets, the unknowns $x = \phi, \mu_n, V_{\mathrm{L}}$, and the observable I_{L}, the linearized small-signal system in block matrix form reads (see [34] for analytical expressions of the functional derivatives)

$$\begin{pmatrix} J_{xx} & 0 \\ J_{Ix} & -1 \end{pmatrix}\begin{pmatrix} \delta x \\ \delta I_{\mathrm{L}} \end{pmatrix} = \begin{pmatrix} \xi_x \\ \xi_{I_{\mathrm{L}}}, \end{pmatrix}, \tag{17}$$

where J_{xx} and J_{Ix} are block components of the frequency-dependent Jacobian matrix. A direct evaluation of all the transfer fields relating the noise fluctuations ξ_α with all the system variables would be computationally inefficient, since for the noise analysis we need only the elements $\mathcal{G}_{I\beta}$ connecting the terminal current fluctuations with unit excitations in the model equations. Originally developed for the sensitivity analysis of circuits, and later applied to noise models of semiconductor devices [11, 45], Branin's method allows to compute the required transfer fields with a negligible overhead with respect to the small-signal analysis. Solving for δx, and substituting in the equation for the current fluctuations, we find

$$\delta I_{\mathrm{L}} = y^{\mathrm{T}}\xi_x - \xi_{I_{\mathrm{L}}}, \tag{18}$$

where the column array y is the solution of the transposed problem

$$J^{\mathrm{T}}_{xx} y = J^{\mathrm{T}}_{Ix}. \tag{19}$$

Comparing (18) with (6), we find the transfer fields required for noise analysis: the elements of y corresponding to the Poisson and continuity equations are the short-circuit transfer fields $\mathcal{G}_{I\phi}$ and $\mathcal{G}_{I\mu_n}$, respectively, $\mathcal{G}_{II} = -1$, and the element of y that corresponds to the voltage V provides the small-signal admittance $\mathcal{G}_{IV}$.

Having computed the transfer fields $\mathcal{G}_{I\beta}$, we now turn our attention to the calculation of the microscopic noise sources ξ_α that appear in the right-hand-side of (13).

Assuming no external noise sources ($\xi_V = 0$), inspection of the fluctuating quantities in (13) gives

$$\xi_\phi^{(i)} = \delta n_i \tag{20a}$$

$$\xi_{\mu_n}^{(i)} = \frac{\delta I_i}{\mathrm{e}\Delta} + \mathrm{i}\omega\delta n_i \tag{20b}$$

$$\xi_{I_\mathrm{L}} = \delta I_\mathrm{L}, \tag{20c}$$

where δI_i and δn_i are the current and charge fluctuations of the Büttiker probes, respectively, and δI_L is the current fluctuation of the left contact. The average current I_i flowing in the i-th Büttiker-probe may be computed as $I_{i,i-1} + I_{i,i+1}$, where $I_{i,i+1}$ is the current flowing between nodes i and $i+1$ [28]

$$I_{i,i+1} = \frac{e}{\hbar}\int \frac{\mathrm{d}E}{2\pi} 2\mathbb{R}\mathrm{e}\left\{H_{i,i+1}G^<_{i+1,i}(E)\right\}. \tag{21}$$

Current conservation implies that I_i must be zero upon integration over energy, but the corresponding operator fluctuates. The fluctuation of $I_{i,i+1}$ is characterized by its spectral density, defined as the Fourier transform of the correlation function (curly brackets indicate anticommutators)

$$\begin{aligned} K_{\delta I_{i,i+1}\delta I_{i,i+1}}(t-t') &= \frac{1}{2}\langle\{\delta I_{i,i+1}(t), \delta I_{i,i+1}(t')\}\rangle \\ &= \langle\{I_{i,i+1}(t), I_{i,i+1}(t')\}\rangle - 2\langle I_{i,i+1}\rangle^2. \end{aligned} \tag{22}$$

Following the procedure for the calculation of quantum statistical averages [23], (22) can be expressed in terms of two-electron Green's functions, which are then approximated as the sum of products of two one-electron Green's functions according to Wick's theorem [25, 26, 28, 46], giving, in the zero-frequency limit (disconnected diagrams exactly canceling $-2\langle I_{i,i+1}\rangle^2$)

$$\begin{aligned} K_{\delta I_{i,i+1}\delta I_{i,i+1}} = \mathrm{e}^2 H_{i,i+1}^2 \int \frac{\mathrm{d}E}{2\pi\hbar} [&G^<_{i,i+1}(E)G^>_{i,i+1}(E) \\ &- G^<_{i+1,i+1}(E)G^>_{i,i}(E) - G^<_{i,i}(E)G^>_{i+1,i}(E) \\ &+ G^<_{i+1,i}(E)G^>_{i+1,i}(E)]. \end{aligned} \tag{23}$$

A more general expression valid at finite frequencies can be found in [25]. In the ballistic limit, when no Büttiker probes break the coherent propagation of the carriers, and in the absence of Coulomb correlation effects, the power spectrum defined in (23) is position-independent and already provides the final result. However, in the presence of phase-breaking processes, or even in the coherent limit when the electrostatic potential is computed self-consistently to account for space-charge effects, the complete set of microscopic noise sources (20) should be defined and propagated to the contacts to recover the Nyquist limit at equilibrium. The noise spectra of these sources may be computed in terms of products of lesser and greater Green's functions following the same approach used to derive (23), but the results are quite lengthy. Moreover, difficulties arise in the integration over the transverse energy that appears in the arguments of the Fermi functions, which are encoded in the correlation Green's functions $G^\lessgtr$. However, the calculation of correlation spectra from the scattering matrix is more transparent and compact, as the unitarity of the scattering matrix expressing current conservation simplifies the derivation [29]. Therefore, we find it more convenient to move to a description based on scattering theory using the Fisher-Lee connection between Keldysh Green's functions and scattering matrices [47, 48],

$$s_{\alpha\beta}(E) = -\delta_{\alpha\beta} + \mathrm{i}\hbar\sqrt{v_\alpha(E)v_\beta(E)}G^R_{\alpha\beta}(E), \tag{24}$$

where the indices α and β run over the physical and scattering terminals of the device, and the group velocities are defined by

$$v_\alpha(E) = \Delta\Gamma_\alpha(E)/\hbar. \tag{25}$$

Then, the zero-frequency power and correlation spectra of the elementary noise sources δI_α and δn_α can be computed from the multiterminal Landauer-Büttiker theory [29]. We define a position- and energy-resolved power spectrum of the current fluctuations in the zero-frequency limit as

$$K_{\delta I_\alpha \delta I_\beta}(E) = \mathrm{e}^2 \sum_{\gamma\delta} A_{\gamma\delta}(\alpha, E)A_{\delta\gamma}(\beta, E)F_{\delta\gamma}(E) \tag{26}$$

with the current matrix elements given by [29]

$$A_{\gamma\delta}(\alpha, E) = \delta_{\alpha\gamma}\delta_{\alpha\delta} - s^*_{\alpha\gamma}(E)s_{\alpha\delta}(E). \tag{27}$$

Within scattering matrix theory, charge fluctuations are usually described in terms of the *local partial density of states*, which can be computed from the change of the scattering matrix due to a local perturbation of the electrostatic potential [49]. However, in the present approach, in which the functional derivatives of the scattering matrix are not immediately available (the Jacobian is expressed in terms of steady-state Green's functions), we prefer to derive the charge fluctuations spectra directly from the field operators introduced in [29], to obtain

$$K_{\delta n_\alpha \delta n_\beta}(E) = \sum_{\gamma\delta} B_{\gamma\delta}(\alpha, E)B_{\delta\gamma}(\beta, E)\mathcal{F}_{\delta\gamma}(E), \tag{28}$$

where the charge matrix elements are defined as

$$\begin{aligned} B_{\gamma\delta}(\alpha, E) = [&\delta_{\alpha\gamma}\delta_{\alpha\delta} + s^*_{\alpha\gamma}(E)s_{\alpha\delta}(E) \\ &+ \delta_{\alpha,\gamma}s_{\alpha\delta}(E) + \delta_{\alpha\delta}s^*_{\alpha\gamma}(E)]/v_\alpha(E), \end{aligned} \tag{29}$$

while for the cross-correlation spectra we find

$$K_{\delta I_\alpha \delta n_\beta}(E) = \mathrm{e}\sum_{\gamma\delta} A_{\gamma\delta}(\alpha, E)B_{\delta\gamma}(\beta, E)\mathcal{F}_{\delta\gamma}(E). \tag{30}$$

All integrals over the transverse energy E_k are now isolated in the factors (a closed form expression can be found

with symbolic integration tools, but it not reported here for brevity)

$$\mathcal{F}_{\delta\gamma}(E) = N_{2D}\int \mathrm{d}E_k \left\{ f_\gamma(E+E_k)[1-f_\delta(E+E_k)] + f_\delta(E+E_k)[1-f_\gamma(E+E_k)] \right\}. \tag{31}$$

Following [50, Ch. 2] we decompose $F_{\delta\gamma}$ in the sum of two terms, a thermal noise component that vanishes at zero temperature

$$\mathcal{F}^{(\mathrm{th})}_{\delta\gamma}(E) = \mathcal{F}_{\gamma\gamma}(E) + \mathcal{F}_{\delta\delta}(E), \tag{32}$$

and a shot noise contribution that vanishes for zero current [51]

$$\mathcal{F}^{(\mathrm{sh})}_{\delta\gamma}(E) = N_{2D}\int \mathrm{d}E_k [f_\gamma(E) - f_\delta(E)]^2. \tag{33}$$

From the energy-resolved spectra of the elementary fluctuations, we can finally evaluate the (coloured) spectra of the microscopic noise sources in (20), which are then substituted in the discretized version of (7), to provide the desired short-circuit current fluctuations

$$S_{II}(\omega) = \sum_{\gamma,\delta} \mathcal{G}_{I\gamma}(\omega) K_{\xi_\gamma\xi_\delta}(\omega) \mathcal{G}^\dagger_{I\delta}(\omega). \tag{34}$$

A similar procedure can be used for the calculation of the open-circuit voltage fluctuations, the two representations being related by the small-signal admittance.

III. RESULTS

According to Landauer–Büttiker scattering theory [29], noise in a ballistic nanostructure is understood as a mix of thermal emission noise from the reservoirs and shot noise due to current partitioning between transmitted and reflected flows. Shot noise is most pronounced when the current results from statistically independent electrons tunneling through a low-transparency barrier, but may be significantly suppressed with respect to the full Poissonian value $2\mathrm{e}I$ in the presence of carrier correlations due to either Fermi statistics, when electrons, under degenerate conditions, are forced to pass through the conductive channels of the nanostructure one by one, or/and long-range Coulomb interactions, if carrier transport is charge-controlled [37].

In application contexts in which quantum effects do not play an essential role, Monte Carlo simulations have been used by many authors [2, 16, 17] to study noise fluctuations in semiconductor devices. Compared to scattering matrix methods, particle-based techniques for the solution of the Boltzmann transport equation have the advantage of including phase-breaking, scattering processes, as well as long-range Coulomb interactions between carriers. Monte Carlo simulations with self-consistent potential profiles computed from Poisson's equation showed that Coulomb correlations are expected to be significant when the nanostructure is long enough compared to the Debye length corresponding to the charge density in the contacts, but not too long with respect to the mean free path (the average distance between scattering events), as the presence of scattering mechanisms reduces Coulomb correlations, washing them out completely when the carrier transport becomes fully diffusive [52]. Moreover, inspection of the different contributions to the autocorrelation function of the instantaneous current fluctuations revealed that the main contribution to noise suppression originates from velocity-number correlations induced by the self-consistent field [17, 53, 54]. The Monte Carlo simulations were performed for a lightly doped active region of a semiconductor sample embedded between two heavily doped contacts injecting carriers in the active region. Quantum corrections were not included (tunneling across the barrier may be considered negligible for this structure).

With the aim to compare our results with these semiclassical studies, we consider a GaAs *n-i-n* diode consisting of a 30 nm intrinsic layer between highly doped contacts. The limited height of the barrier and a contact doping of $10^{18}\ \mathrm{cm}^{-3}$ ensures the degeneracy injection necessary to observe the interplay of Fermi and Coulomb correlations. Restricting our attention to the zero-frequency limit, we partition the microscopic noise sources (20) into two sets, the first including current fluctuations at physical and scattering terminals (corresponding to the diffusion noise sources due to velocity fluctuations in the DD formalism), and the second one including only charge fluctuations (absent in DD-based noise models). Then, we can decompose the total current noise spectrum S_{II} into three contributions

$$S_{vv} = \sum_{\gamma,\delta=\mu_n,I} \mathcal{G}_{I\gamma} K_{\xi_\gamma\xi_\delta} \mathcal{G}^\dagger_{I\delta} \tag{35a}$$

$$S_{vn} = \sum_{\gamma=\mu_n,I} 2\mathbb{R}\mathrm{e}\left\{ \mathcal{G}_{I\phi} K_{\xi_\phi\xi_\gamma} \mathcal{G}^\dagger_{I\gamma} \right\} \tag{35b}$$

$$S_{nn} = \mathcal{G}_{I\phi} K_{\xi_\phi\xi_\phi} \mathcal{G}^\dagger_{I\phi}, \tag{35c}$$

corresponding to current, current-density and density correlations, respectively. Fig. 1a shows the decomposition of the zero-frequency current noise spectrum as a function of the applied bias. All spectra are normalized with respect to the equilibrium thermal noise $S_{\mathrm{eq}} = 4k_{\mathrm{B}}TG_{\mathrm{eq}}$, G_{eq} being the small-signal conductance at equilibrium. Also shown for reference is the Poissonian power spectrum computed with the conventional expression used to describe the crossover from thermal to shot noise [55, Ch. 6]

$$S_P = 2\mathrm{e}I \coth\left(\frac{\mathrm{e}V}{2k_{\mathrm{B}}T}\right). \tag{36}$$

At equilibrium, the Nyquist limit is recovered with machine precision accuracy, which represents a stringent test for any microscopic noise model. For this fundamental

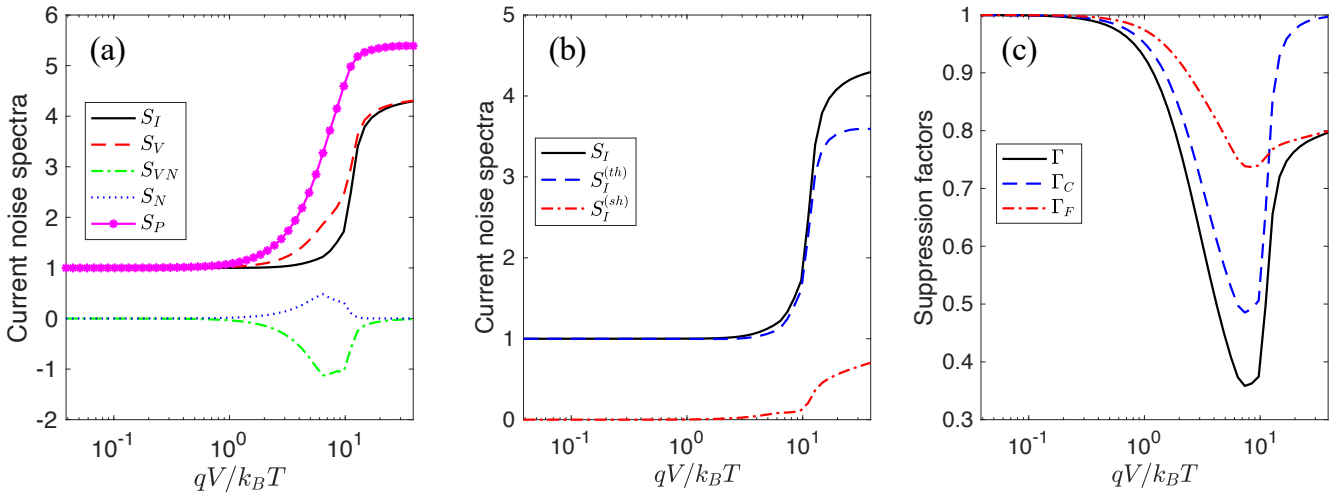


FIG. 1. (a) Decomposition of the zero-frequency current noise spectrum (solid black line) of the *n*-*i*-*n* diode into velocity (dashed red line), velocity-number (dashed-dotted green line), and number-number (blue dots) contributions versus applied voltage. The Poissonian expression (36) is also shown for reference (magenta dots). (b) Thermal (dashed blue curve) and shot noise (dashed-dotted red curve) components of the current noise (solid black line). (c) Current noise suppression factors $\Gamma_{\rm C}$, $\Gamma_{\rm F}$, and $\Gamma = \Gamma_{\rm C}\Gamma_{\rm F}$, computed as a function of the applied bias. All calculations were performed at room temperature. Spectra are normalized with respect to the equilibrium thermal noise.

law to hold exactly, the Jacobian matrix must be complete and accurate, and the transfer fields must be well defined also at the boundaries, which lead us to reformulate the current conserving boundary conditions introduced in [34] as discussed in Section II. For low applied voltages, the overall current noise spectrum can be entirely ascribed to local current fluctuations, as density and current-density fluctuations are not propagated by the equilibrium transfer fields (from a Monte Carlo perspective, S_{nn} and S_{vn} are zero at equilibrium because they are both proportional to the average velocity [52]). At higher applied voltages, both S_{nn} and S_{vn} contribute to the total noise with opposite signs, their magnitude peaking just before the current saturation [56].

The contribution S_{vn} due to current-density correlations is negative and only partially compensated by S_{nn}, leading to noise suppression, in agreement with [17]. When the coherent limit is approached, our NEGF calculations are also in agreement with analytical results based on the solution of Vlasov's equation (the collisionless Boltzmann transport equation) with a self-consistent field: for lower scattering strengths, the noise spectrum S_{II} is suppressed below the equilibrium Nyquist limit predicted by the fluctuation-dissipation theorem, a condition known as "negative excess noise" [37, 57].

The current spectrum may also be decomposed in thermal and shot noise components according to the definitions (32) and (33). At low applied voltages, the thermal component dominates, converging to the Nyquist limit at equilibrium, while the shot-noise component becomes significant when the current starts to saturate, see Fig. 1b.

In order to disentangle Fermi and Coulomb correlations, we fix the electrostatic potential in the calculation of the transfer fields by setting to zero the corresponding off-diagonal blocks in the Jacobian matrix in (19). Defining $S_{II}^{(\rm uncor)}$ as the current spectrum obtained by switching off Coulomb interactions, we introduce the suppression factors

$$\Gamma_{\rm F} = S_{II}^{(\rm uncor)}/S_P \tag{37a}$$

$$\Gamma_{\rm C} = S_{II}/S_{II}^{(\rm uncor)} \tag{37b}$$

due to Fermi and Coulomb correlations, respectively. Fig. 1c shows $\Gamma_{\rm F}$, $\Gamma_{\rm C}$, and the total suppression factor $\Gamma = \Gamma_{\rm C}\Gamma_{\rm F}$ as a function of the applied bias. While $\Gamma_{\rm F}$ decreases almost monotonically, $\Gamma_{\rm C}$ exhibits a more pronounced minimum, after which it increases approaching unity as the potential barrier disappears under saturation conditions when space-charge effects do not modulate anymore the random injection of the carriers from the contacts [17], in qualitative agreement with analytical results obtained from the solution of the collisionless Boltzmann equation coupled with Poisson's equation and complemented with stochastic boundary conditions [37].

Coulomb correlations usually lead to shot noise suppression, but enhancement is also possible in the presence of a negative differential conductivity (NDC) region. As an example, we consider the resonant tunneling diode (RTD) studied in [34], consisting of a 5 nm $In_{0.53}Ga_{0.47}As$ quantum well between 1.5 nm-thick AlAs barriers. The intrinsic double-barrier quantum well heterostructure is embedded in lightly doped spacer layers (20 nm, $N_{\rm D} = 10^{17}\,{\rm cm}^{-3}$), followed by heavily doped contact layers (20 nm, $N_{\rm D} = 10^{19}\,{\rm cm}^{-3}$). If the RTD is biased in the NDC region, when the resonant energy is falling below the conduction band at the emitter contact, the presence of one electron inside the quantum well

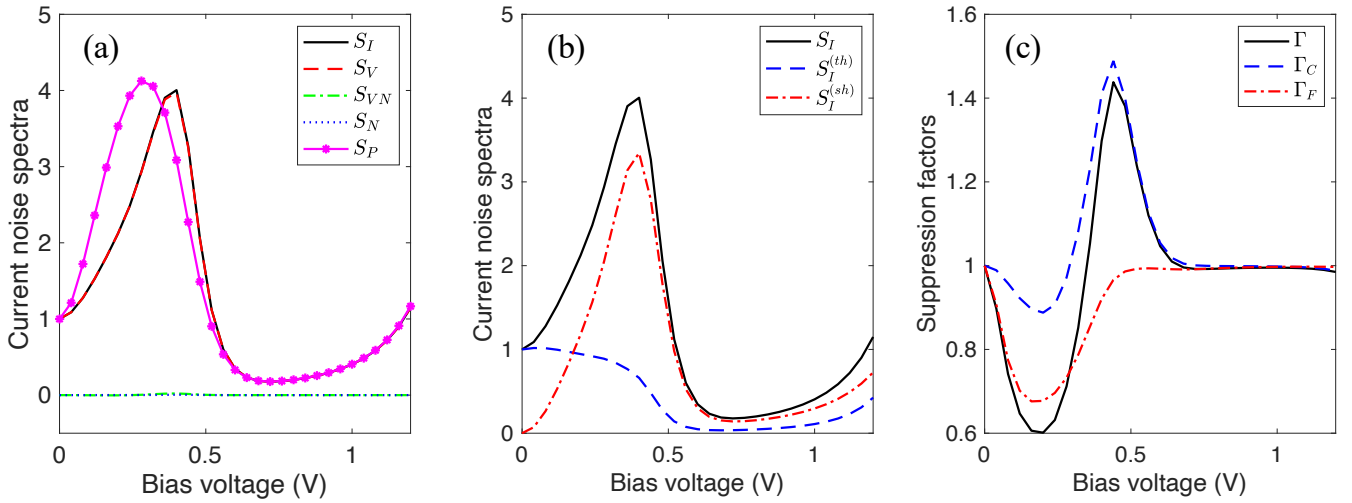


FIG. 2. (a) Decomposition of the (normalized) current noise spectrum (solid black curve) of the RTD structure into velocity (dashed red curve), velocity-number (dashed-dotted green curve) and number-number (blue dots) contributions versus applied voltage. Expression (36) is reported for reference (magenta dots). (b) Thermal and shot noise components of the current noise. (c) Current noise suppression factors $\Gamma_{\rm C}$, $\Gamma_{\rm F}$, and $\Gamma = \Gamma_{\rm C}\Gamma_{\rm F}$ computed as a function of the applied bias.

raises the potential energy of the well, thus facilitating the crossing of other electrons [58]. The electrons crossing the barrier are therefore positively correlated, leading to a Fano factor higher than one, i.e., super-Poissonian noise. On the other hand, if the structure is biased before the resonant peak, the presence of an electron inside the quantum well obstructs the transport of the second one, leading to sub-Poissonian noise.

Fig. 2a shows that the contributions S_{nn} and S_{vn} are negligible over the whole bias range, as expected from the low average carrier velocity in the nanostructure. In the NDC region, where carrier transport across the barrier is assisted by phonon scattering, shot noise dominates, while beyond the resonance peak, where Fermi and Coulomb correlations are absent, both thermal and shot noise components contribute to reach the Poissonian value (36), see Fig. 2b. The negligible role of number fluctuations does not imply that Coulomb correlations are absent, since space-charge effects are encoded in $\mathcal{G}_{I\mu_n}$. The suppression factors $\Gamma_{\rm C}$, $\Gamma_{\rm F}$, and Γ are shown in Fig. 2c as a function of the applied voltage. Notice that $\Gamma_{\rm F}$ remains always less than one (dashed-dotted red line), i.e., there is no noise enhancement in the absence of Coulomb correlations, in agreement with analytical calculations based on capacitance models [58] and quantum simulations based on Bohm trajectories [59].

Inspection of the relevant spectrally resolved observables and transfer fields provides insight in the origin of the noise enhancement. Fig. 3a shows the spectral current computed for $V_{\rm bias} = 0.4\,{\rm V}$ in the NDC region. The sudden interruption in the otherwise almost coherent propagation of the electrons is indicative of sequential tunneling assisted by phonon emission processes [34]. The power spectra of the local current fluctuations away from the average are represented in Fig. 3b. While the average current flows mostly at the energy of the bound state, fluctuations in the Büttiker-probe currents can be noticed below the Fermi window on both sides of the quantum well. The transfer fields $\mathcal{G}_{I_{\rm L}\mu_n}$, $\mathcal{G}_{I_R\mu_n}$ propagating the local current fluctuations to the contacts, computed with (solid lines) and without (dashed lines) space-charge effects, are shown in Fig. 3c. In the non-self-consistent case, the transfer fields are always bounded in the interval [-1,0].

If the nanostructure is designed to absorb an optical signal, we may interpret $\mathcal{G}_{I_{\rm L}\mu_n}$ ($\mathcal{G}_{I_R\mu_n}$) as the probability that a carrier photogenerated at a specific point in the detector is collected by the contact on the left (right), contributing to the photocurrent after diffusion. In the self-consistent calculation, the transfer fields exceed the interval [-1,0] within the quantum well, meaning that a current pulse injected in the well will be collected by the right contact, but it will also induce an electron flow from the left contact, providing a current gain. In both cases, with and without space-charge effects, the sum of the two transfer fields associated to the left and right contacts is always equal to -1, expressing current conservation. In conclusion, shot noise enhancement due to Coulomb correlations is indicative of an internal gain mechanism when a current fluctuation is injected into the structure. Indeed, photodetectors based on resonant tunneling structures operating at relatively low applied voltages have been proposed as an alternative architecture to avalanche photodetectors for the detection of weak or even single-photon infrared signals [60].

One of the original motivations for noise analysis has been its potential to evaluate the strength and nature of the scattering processes acting in the nanostructure. The coherent and scattering components of the current noise spectra cannot be unambiguously separated, since the

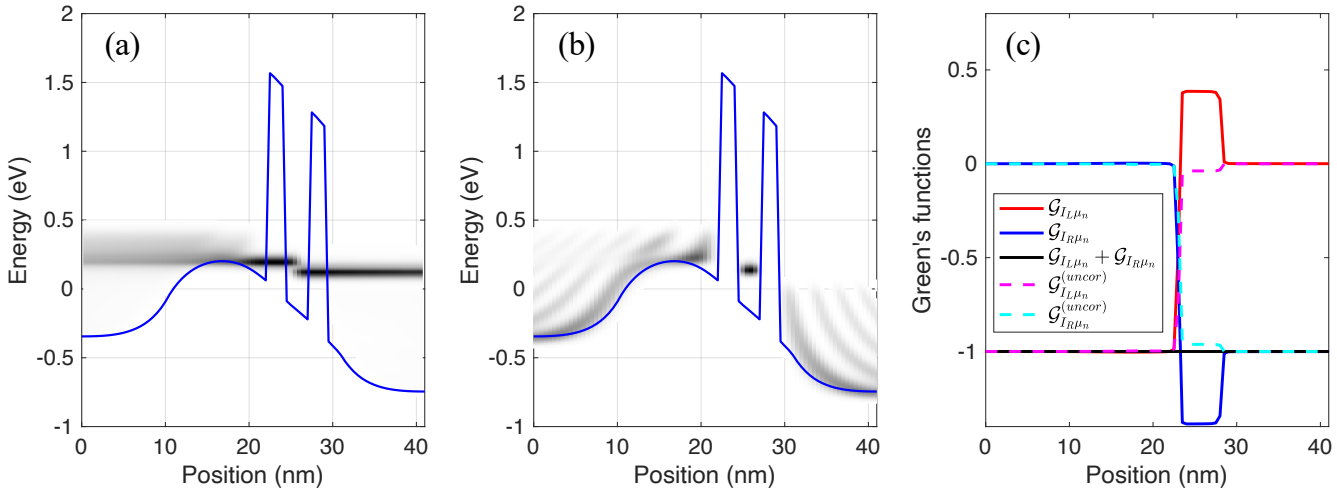


FIG. 3. (a) Spectral current density (grayscale maps) computed for $V = 0.4\,\mathrm{V}$ in the NDC region. (b) Noise spectra of the microscopic noise sources $K_{\delta I_\alpha \delta I_\alpha}(E)$ describing the current fluctuations in the Büttiker probes. Only the power spectra of the fluctuations are shown, but cross correlations between different probes (negative for a system of fermions [29]) exist up to a distance of few nanometers. (c) Transfer fields describing the current response at the terminals due to a unit, spatially impulsive current injected in the electron continuity equation, with Coulomb correlations (solid lines) and in frozen field conditions (dashed lines). The self-consistent transfer fields indicate a current gain for current injection in the quantum well.

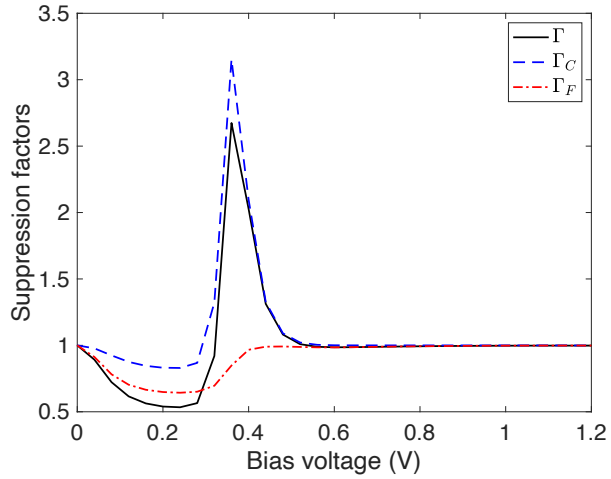


FIG. 4. Current noise Fano factors Γ_C, Γ_F, and $\Gamma = \Gamma_C\Gamma_F$ computed as a function of the applied bias for the RTD with polar optical phonon scattering strength artificially decreased by a factor of four. Approaching the coherent limit, the noise enhancement due to Coulomb correlations is more pronounced.

microscopic noise sources associated with the Büttiker probes (used for the description of the scattering processes) and with the physical contacts (the only noise sources that survive in the coherent limit) are spatially correlated. So, we follow the conventional approach of looking for signatures of scattering in the Fano factor. As sequential tunneling assisted by optical phonons is the dominant transport mechanism in the NDC region of the RTD [34], it is not surprising that the Fano factor is mostly affected in this region by polar optical scattering, while (elastic) acoustic phonon scattering plays a negligible role. A strong enhancement of the Fano factor Γ_C associated with Coulomb correlations can be observed if the scattering strength is artificially decreased by a factor of four, see Fig. 4. This result is consistent with the expectation that the action of inelastic scattering mechanisms tends to counteract the effect of self-consistent field fluctuations [52]. The noise enhancement observed when the coherent limit is approached is also partially related to the noiseless DC working point [61], as a reduced scattering-induced broadening leads to a more pronounced resonance in the I-V characteristics compared to fully scattered simulations [34].

So far we have presented zero-frequency current noise spectra. Fig. 5 shows the equilibrium voltage noise spectrum (red line) of the RTD under study computed as a function of the AC driving frequency ω. As expected, the equilibrium noise provides the same information of the small-signal analysis: the Nyquist limit (not shown for clarity) is superimposed to the calculated spectrum at all frequencies. Although the elementary noise sources (26), (28), and (30) are white, the resulting current noise spectrum is colored, due to the dependence of Langevin forces and transfer fields on frequency. A circuit representation of the small-signal impedance of the RTD, see e.g., [62, 63], suggests a simple interpretation of the noise frequency behavior. The adopted equivalent circuit model includes the contact resistance R_s in series with the parallel combination of the (intrisic) RTD capacitance C_n and conductance G_n. The conductance G_n dominates the real part of the low frequency impedance (and consequently the equilibrium voltage noise spectrum) up to

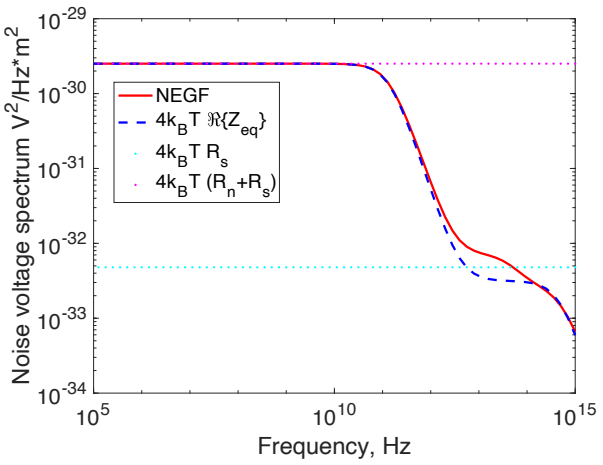


FIG. 5. Equilibrium voltage noise spectrum of the resonant tunnelling diode obtained from the present approach (red line), and from the small-signal impedance $Z_{\rm eq}$ of the equivalent circuit (blue dashed line). The cyan and magenta dotted lines represent the thermal noise associated to R_s and R_n+R_s, respectively ($R_n = 1/G_n$). The circuit parameters were extracted from the NEGF small-signal impedance.

the corner frequency $f = 1/(2R_nC_n) \approx 0.2\,\mathrm{THz}$, beyond which the intrinsic part of the device is short-circuited by C_n. In the high-frequency limit, the noise spectrum should converge to the thermal contribution of the series resistance, but a clear saturation of the noise spectrum to $4k_{\rm B}TR_s$ could not be observed due to the presence of the dielectric capacitance C_d in parallel with the equivalent circuit of the RTD (the simulation window employed in the NEGF simulation of the RTD was just few tens of nanometer wide due to computational restrictions).

The noise spectrum is shown for completeness up to $10^{15}\,\mathrm{Hz}$, but the small-signal model used for the calculation of the transfer fields is valid only at sub-terahertz frequencies due to simplifications adopted to the avoid the difficulties arising from the two-times structure of the NEGF formalism [34]. A more rigorous treatment would require a formalism based on a double-time Fourier transform, in which the matrix elements (27) and (29) are evaluated from the product of two scattering matrices at different energies, E and $E + \hbar\omega$ [64]. While this more rigorous approach accounts for the generation of sidebands in the Green's functions at integer multiples of the driving frequency (photon-assisted tunnelling), it represents a significant departure from the simplified small-signal model proposed in [34]. Therefore, in analogy with impedance-field noise calculations based on the DD formalism [65, 66], we adopt zero-frequency expressions for the spectra of the elementary noise sources. The proposed NEGF formulation provides a more fundamental description of noise sources and transfer fields with respect to DD schemes, but a significant extension of the formalism presented here would be required to perform a study of the corner frequencies associated with the different scattering mechanisms. We will postpone this analysis to a future work.

IV. CONCLUSION

We have presented a unified description of carrier transport and noise properties of semiconductor nanostructures within the NEGF formalism. With respect to conventional impedance-field approaches based on the drift-diffusion approximation [11], the microscopic noise sources associated to intraband scattering processes are computed in a consistent way, directly from the Green's functions, rather than being postulated in homogeneous bulk conditions neglecting spatial correlations. In agreement with Monte Carlo simulations, the proposed model shows that shot-noise suppression due to long-range Coulomb interactions may persist in a wide range of applied voltages under quasi-ballistic conditions, which represents a common scenario in modern nanodevices.

Possible applications include noise analysis in highly nanostructured optoelectronic devices such as T2SL infrared photodetectors, in which different transport regimes such as miniband propagation, sequential tunneling and Wannier-Stark hopping may coexist [67, 68]. As generation/recombination processes are treated in the present NEGF model by including appropriate semiclassical rates in the continuity equations [33], the additional microscopic noise sources needed to describe interband transitions may be evaluated in the same way as population fluctuations in DD models [12, Ch. 1]. Noise in infrared T2SL detectors is usually investigated by means of empirical approaches based on the Hooge model, in which the noise spectra are obtained by superimposing different current contributions (diffusion, SRH, trap-assisted tunneling, and band-to-band tunneling) with appropriate fitting parameters to reproduce the observed dependence on temperature and bias [8, 69, 70]. The detectivity of infrared imaging systems is ultimately limited by the excess noise above the shot noise floor, which may lead to frequent calibrations of the detector or pixel blinking in the presence of random telegraph noise. The proposed NEGF model should provide a more physically sound perspective on the origin of microscopic fluctuations and their propagation in T2SL detectors.

Finally, the small-signal transfer fields derived in this work can be used to study the variability of nanostructures due to structural and compositional variations [71, 72].

ACKNOWLEDGMENT

The authors are deeply indebted to Tomáš Novotný for interesting discussions and suggestions. This work was supported by the Office of Naval Research Global (award number N629092412059), and by the European Union, through two initiatives of the Italian National

Recovery and Resilience Plan (NRRP) of NextGenerationEU: the PRIN Project 20225YYLEP, 'Empowering UV Led technologies for high-efficiency disinfection: from semiconductor-level research to SARs-Cov-2 inactivation', Mission 4, Component C2, Investment 1.1, and the National Centre for HPC, Big Data and Quantum Computing under Grant CN00000013 - CUP E13C22000990001.

[1] R. Landauer, "The noise is the signal," *Nature*, vol. 392, pp. 658–659, Apr. 1998.

[2] L. Varani, L. Reggiani, T. Kuhn, T. Gonzaléz, and D. Pardo, "Microscopic simulation of electronic noise in semiconductor materials and devices," *IEEE Trans. Electron Devices*, vol. ED-41, no. 11, pp. 1916–1925, Nov. 1994.

[3] V. Nam Do, P. Dollfus, and V. Lien Nguyen, "Phonon-induced shot noise enhancement in resonant tunneling structures," *Appl. Phys. Lett.*, vol. 91, no. 2, p. 022104, 2007.

[4] D. Li, L. Zhang, F. Xu, and J. Wang, "Enhancement of shot noise due to the fluctuation of Coulomb interaction," *Phys. Rev. B*, vol. 85, no. 16, p. 165402, 2012.

[5] B. H. Wu, J. C. Cao, and K.-H. Ahn, "Reduction of shot noise in superlattice structures by nonequilibrium Green's function calculations," *Phys. Rev. B*, vol. 74, no. 19, p. 195316, 2006.

[6] W. Song, A. K. M. Newaz, J. K. Son, and E. E. Mendez, "Reduction of shot noise in superlattice structures by nonequilibrium Green's function calculations," *Phys. Rev. Lett.*, vol. 96, no. 12, p. 126803, 2006.

[7] B. H. Wu and J. C. Cao, "Keldysh Green's function approach to the noise properties of semiconductor superlattices," *Physica E*, vol. 40, no. 5, pp. 1319–1321, 2008.

[8] Ł. Ciura, A. Kolek, J. Jureńczyk, K. Czuba, A. Jasik, I. Sankowska, and J. Kaniewski, "$1/f$ noise modeling of InAs/GaSb superlattice mid-wavelength infrared detectors," *Opt. Quantum Electron.*, vol. 50, p. 36, 2018.

[9] E. A. Garduño, V. M. Cowan, G. D. Jenkins, C. P. Morath, and E. H. Steenbergen, "Comparison of pre-and post-irradiation low-frequency noise spectra of midwave infrared nBn detectors with superlattice absorbers," *IEEE Trans. Nucl. Sci.*, vol. 64, no. 4, pp. 1042–1047, 2017.

[10] N. I. Bochkareva, A. M. Ivanova, A. V. Klochkova, and Y. G. Shretera, "Current noise and efficiency droop of light-emitting diodes in defect-assisted carrier tunneling from an InGaN/GaN quantum well," *Semicond.*, vol. 53, no. 1, pp. 99–105, Jan. 2019.

[11] F. Bonani, G. Ghione, M. R. Pinto, and R. K. Smith, "An efficient approach to noise analysis through multidimensional physics-based models," *IEEE Trans. Electron Devices*, vol. 45, no. 1, pp. 261–269, 1998.

[12] F. Bonani and G. Ghione, *Noise in Semiconductor Devices. Modeling and Simulation*, ser. Advanced Microelectronics. Berlin: Springer-Verlag, 2001.

[13] E. Starikov, P. Shiktorov, V. Gružinskis, T. Gonzáles, M. J. Martín, D. Pardo, L. Reggiani, and L. Varani, "Hydrodynamic and Monte Carlo simulation of steady-state transport and noise in submicrometre n^+nn^+ silicon structures," *Semiconductor Sci. Technol.*, vol. 11, no. 6, pp. 865–872, 1996.

[14] C. Jungemann and B. Meinerzhagen, *Hierarchical Device Simulation. The Monte-Carlo Perspective*, ser. Computational Microelectronics. Wien: Springer-Verlag, 2003.

[15] C. Jungemann, "The Langevin-Boltzmann equation for noise calculation," in *Noise in Nanoscale Semiconductor Devices*, T. Grasser, Ed. Cham, Switzerland: Springer, 2020, ch. 19, pp. 649–685.

[16] T. Kuhn, L. Reggiani, L. Varani, and V. Mitin, "Monte Carlo method for the simulation of electronic noise in semiconductors," *Phys. Rev. B*, vol. 42, no. 9, pp. 5702–5713, Sep. 1990.

[17] T. González, O. M. Bulashenko, J. Mateos, D. Pardo, and L. Reggiani, "Effect of long-range Coulomb interaction on shot-noise suppression in ballistic transport," *Phys. Rev. B*, vol. 56, no. 11, p. 6424, 1997.

[18] M. Fischetti and W. G. Vandenberghe, *Advanced Physics of Electron Transport in Semiconductors and Nanostructures*. Berlin: Springer-Verlag, 2016.

[19] Case in point are antimonide-based T2SLs, which are recently emerging as a possible alternative to the well-established infrared imaging technology based on mercury cadmium telluride [73]. While vertical mobilities and minority carrier lifetimes determine the collection efficiency, the excess noise above the shot noise floor ultimately limits the detectivity of the infrared imaging system, which may lead to frequent calibrations, or even pixel blinking in the presence of random telegraph noise [74].

[20] M. Luisier, "Atomistic simulation of transport phenomena in nanoelectronic devices," *Chem. Soc. Rev.*, vol. 43, no. 13, pp. 4357–4367, 2014.

[21] C. Jirauschek and T. Kubis, "Modeling techniques for quantum cascade lasers," *Appl. Phys. Rev.*, vol. 1, no. 1, p. 011307, 2014.

[22] U. Aeberhard, "Photovoltaics at the mesoscale: insights from quantum-kinetic simulation," *J. Phys. D*, vol. 51, no. 32, p. 323002, 2018.

[23] F. M. Souza, A. P. Jauho, and J. C. Egues, "Spin-polarized current and shot noise in the presence of spin flip in a quantum dot via nonequilibrium Green's functions," *Phys. Rev. B*, vol. 78, no. 15, p. 155303, 2008.

[24] H. Haug and A.-P. Jauho, *Quantum Kinetics in Transport and Optics of Semiconductors*, 2nd ed. Berlin: Springer, 2008.

[25] Z. Wang, M. Iwanaga, and T. Miyoshi, "Current noise in semiconductor quantum dots," *Jpn. J. Appl. Phys.*, vol. 37, no. 11R, pp. 5894–5901, 1998.

[26] A.-P. Jauho, "Nonequilibrium Green's function modelling of transport in mesoscopic systems," in *Progress in Nonequilibrium Green's Functions II*, Dresden, Germany, Aug. 2002.

[27] J.-X. Zhu and A. V. Balatsky, "Theory of current and shot-noise spectroscopy in single-molecular quantum dots with a phonon mode," *Phys. Rev. B*, vol. 67, no. 16, p. 165326, 2003.

[28] T. Miyoshi, H. Tsuchiya, M. Ogawa, A. Asanuma, and T. Okauchi, "Current noise in semiconductor nanoscale

devices," in *Proc. SPIE 5470*, May 2004, pp. 28–36.
[29] M. Büttiker, "Scattering theory of current and intensity noise correlations in conductors and wave guides," *Phys. Rev. B*, vol. 46, no. 19, p. 12485, 1992.
[30] F. Haupt, T. Novotný, and W. Belzig, "Current noise in molecular junctions: Effects of the electron-phonon interaction," *Phys. Rev. B*, vol. 82, no. 16, p. 165441, 2010.
[31] L. Levitov and G. B. Lesovik, "Charge-transport statistics in quantum conductors," *JETP Lett.*, vol. 55, no. 9, pp. 555–559, 1992.
[32] T. Novotný, "Full counting statistics of electronic transport through interacting nanosystems," *J. Comp. Electron.*, vol. 12, pp. 375–387, 2013.
[33] A. Tibaldi, J. A. Gonzalez Montoya, M. Vallone, M. Goano, E. Bellotti, and F. Bertazzi, "Modeling infrared superlattice photodetectors: From nonequilibrium Green's functions to quantum-corrected drift diffusion," *Phys. Rev. Appl.*, vol. 16, no. 4, p. 044024, Oct. 2021.
[34] A. Tibaldi, M. Goano, and F. Bertazzi, "Small-signal modeling of dissipative carrier transport in nanodevices with nonequilibrium Green's functions," *Phys. Rev. Appl.*, vol. 19, no. 6, p. 064020, Jun. 2023.
[35] J.-P. Nougier, "Fluctuations and noise of hot carriers in semiconductor materials and devices," *IEEE Trans. Electron Devices*, vol. 41, no. 11, pp. 2034–2049, 1994.
[36] H.-H. Park and G. Klimeck, "Quantum approach to electronic noise calculations in the presence of electron-phonon interactions," *Phys. Rev. B*, vol. 82, no. 12, p. 125328, 2010.
[37] O. M. Bulashenko and J. M. Rubí, "Self-consistent theory of current and voltage noise in multimode ballistic conductors," *Phys. Rev. B*, vol. 66, no. 4, p. 045310, 2002.
[38] W. Kausel, G. Nanz, S. Selberherr, and H. Poetzl, "A new boundary condition for device simulation considering outer components," in *Simulation of Semiconductor Devices and Processes*, vol. 3, Bologna, Sep. 1988, pp. 625–636.
[39] A finite-element discretization of the NEGF equations would provide better accuracy, especially in the presence of material and doping discontinuities, but for clearness, we favor a finite-difference scheme, since the use of a non-orthogonal set of basis functions would lead to lengthy expressions of the Jacobian matrix.
[40] A simple matrix transformation allows the use of nonuniform meshes preserving the symmetries of the Green's functions [75].
[41] J. A. Vaitkus and J. H. Cole, "Büttiker probes and the recursive Green's function: an efficient approach to include dissipation in general configurations," *Phys. Rev. B*, vol. 97, no. 8, p. 085149, 2018.
[42] Artefacts related to the coherent injection of carriers are undesirable in small-signal calculations, since the frequency response may be controlled by the contacts rather than by the device itself [34].
[43] J. Velev and W. Butler, "On the equivalence of different techniques for evaluating the Green function for a semi-infinite system using a localized basis," *J. Phys. Condens. Matter*, vol. 16, no. 21, pp. R637–R657, 2004.
[44] J. A. Gonzalez Montoya, A. Tibaldi, C. De Santi, M. Meneghini, M. Goano, and F. Bertazzi, "Nonequilibrium Green's function modeling of trap-assisted tunneling in $In_xGa_{1-x}N$/GaN light-emitting diodes," *Phys. Rev. Appl.*, vol. 16, no. 4, p. 044023, Oct. 2021.
[45] S. Donati Guerrieri, M. Pirola, and F. Bonani, "Concurrent efficient evaluation of small-change parameters and Green's functions for TCAD device noise and variability analysis," *IEEE Trans. Electron Devices*, vol. 64, no. 3, pp. 1269–1275, Mar. 2017.
[46] R. López, R. Aguado, and G. Platero, "Shot noise in strongly correlated double quantum dots," *Phys. Rev. B*, vol. 69, no. 23, p. 235305, 2004.
[47] L. Arrachea and M. Moskalets, "Relation between scattering-matrix and Keldysh formalisms for quantum transport driven by time-periodic fields," *Phys. Rev. B*, vol. 74, no. 24, p. 245322, 2006.
[48] C. Jin, J. Lan, X. Zhaoa, and W. Sui, "Mode-detailed analysis of transmission based directly on Green's functions," *Eur. Phys. J. B*, vol. 89, p. 187, 2016.
[49] M. Büttiker, "Charge densities and charge noise in mesoscopic conductors," *Pramana – J. Phys.*, vol. 58, no. 2, pp. 241–257, Feb. 2002.
[50] M. V. Moskalets, *Scattering matrix approach to non-stationary quantum transport*, 1st ed. London: Imperial College Press, 2012.
[51] This somewhat arbitrary decomposition was also adopted in the original two-terminal Landauer-Büttiker formula valid in the non-interacting limit, to distinguish between "quasi-equilibrium" and "transport" noise components [29].
[52] T. González, O. M. Bulashenko, J. Mateos, D. Pardo, L. Reggiani, and J. M. Rubí, "Noise suppression due to long-range Coulomb interaction: crossover between diffusive and ballistic transport regimes," *Semiconductor Sci. Technol.*, vol. 12, no. 8, pp. 1053–1056, 1997.
[53] T. González and D. Pardo, "Ensemble Monte Carlo with Poisson solver for the study of current fluctuations in homogeneous GaAs structures," *J. Appl. Phys.*, vol. 73, no. 11, pp. 7453–7464, Jun. 1993.
[54] T. González, J. Mateos, D. Pardo, O. M. Bulashenko, and L. Reggiani, "Microscopic analysis of shot-noise suppression in nondegenerate ballistic transport," *Semiconductor Sci. Technol.*, vol. 13, no. 7, pp. 714–724, 1998.
[55] A. van der Ziel, Ed., *Noise in Solid State Devices and Circuits*. New York, USA: John Wiley & Sons, 1986.
[56] From a Monte Carlo perspective, current saturation in a quasi-ballistic *n-i-n* diode takes place when all carriers injected from one contact reach the opposite one, while none of the carriers injected from the other contact can cross the nanostructure. The value of the saturation current is independent of the sample length as it is only determined by the emission properties of the contacts [54]. A maximum current may also be defined within the NEGF formalism from the Landauer-Büttiker formula. Both contacts inject thermal fluxes of carriers from both sides of the nanostructure, but for high biases, when the potential barrier of the n-i-n diode has already disappeared and the reflection probability is close to zero, the current is entirely controlled by the contact with the higher Fermi level. This value represents an upper limit since scattering usually reduces the value of the current and unit transmission probabilities are precisely attained only at resonances.
[57] O. M. Bulashenko and J. M. Rubí, "Negative excess noise in ballistic conductors," *Physica E*, vol. 17, pp. 638–639, Apr. 2003.
[58] G. Iannaccone, G. Lombardi, M. Macucci, and B. Pellegrini, "Enhanced shot noise in resonant tunneling: The-

ory and experiment," *Phys. Rev. Lett.*, vol. 80, no. 5, pp. 1054–1057, Feb. 1998.

[59] X. Oriols, "Shot noise in mesoscopic systems within the first quantization formalism: A De Broglie-Bohm wave-particle description," *AIP Conf. Proc.*, vol. 800, no. 1, pp. 171–176, Nov. 2005.

[60] B. Nie, J. Huang, C. Zhao, W. Huang, Y. Zhang, Y. Cao, and W. Ma, "InAs/GaSb superlattice resonant tunneling diode photodetector with InAs/AlSb double barrier structure," *Appl. Phys. Lett.*, vol. 114, no. 5, p. 053509, Feb. 2019.

[61] In general, the noiseless DC working point around which the small-signal noise analysis is performed depends on the scattering processes in a complex way, as the scattering self-energies and the Green's functions are computed self-consistently. When space-charge effects are included by solving Poisson's equation, the scattering processes also change the band diagram. For example, band bending in the quasi-neutral regions is usually associated with dissipative carrier transport. Inelastic scattering processes are also necessary to populate the states that cannot be reached otherwise from the contacts.

[62] R. Lake and J. Yang, "A physics based model for the RTD quantum capacitance," *IEEE Trans. Electron Devices*, vol. 50, no. 3, pp. 785–789, Mar. 2003.

[63] R. Morariu, J. Wang, A. C. Cornescu, A. Al-Khalidi, A. Ofiare, J. M. L. Figueiredo, and E. Wasige, "Accurate small-signal equivalent circuit modeling of resonant tunneling diodes to 110 GHz," *IEEE Trans. Microwave Theory Tech.*, vol. 67, no. 11, pp. 4332–4340, 2019.

[64] Y. M. Blanter and M. Büttiker, "Shot noise in mesoscopic conductors," *Phys. Rep.*, vol. 336, no. 1–2, pp. 1–166, 2000.

[65] F. Bonani, S. Donati Guerrieri, and G. Ghione, "Compact conversion and cyclostationary noise modeling of pn-junction diodes in low-injection. part I. Model derivation," *IEEE Trans. Electron Devices*, vol. 51, no. 3, pp. 467–476, Mar. 2004.

[66] ——, "Compact conversion and cyclostationary noise modeling of pn-junction diodes in low-injection. part II. Discussion," *IEEE Trans. Electron Devices*, vol. 51, no. 3, pp. 477–485, Mar. 2004.

[67] A. Wacker, "Semiconductor superlattices: a model system for nonlinear transport," *Phys. Rep.*, vol. 357, no. 1, pp. 1–111, 2002.

[68] F. Bertazzi, A. Tibaldi, M. Goano, J. A. Gonzalez Montoya, and E. Bellotti, "Non-equilibrium Green's function modeling of type-II superlattice detectors and its connection to semiclassical approaches," *Phys. Rev. Appl.*, vol. 14, no. 1, p. 014083, Jul. 2020.

[69] Ł. Ciura, A. Kolek, J. Jureńczyk, K. Czuba, A. Jasik, I. Sankowska, E. Papis-Polakowska, and J. Kaniewski, "Noise-current correlations in InAs/GaSb type-II superlattice midwavelength infrared detectors," *IEEE Trans. Electron Devices*, vol. 63, no. 12, pp. 4907–4912, Dec. 2016.

[70] D. Ramos, M. Delmas, R. Ivanov, L. Höglund, E. Costard, P.-E. Hellström, and G. Malm, "$1/f$ noise and dark current correlation in midwave InAs/GaSb type-II superlattice IR detectors," *Phys. Status Solidi A*, vol. 218, no. 3, p. 2000557, Sep. 2020.

[71] S. Donati Guerrieri, F. Bonani, F. Bertazzi, and G. Ghione, "A unified approach to the sensitivity and variability physics-based modeling of semiconductor devices operated in dynamic conditions. Part I: Large-signal sensitivity," *IEEE Trans. Electron Devices*, vol. 63, no. 3, pp. 1195–1201, 2016.

[72] ——, "A unified approach to the sensitivity and variability physics-based modeling of semiconductor devices operated in dynamic conditions. Part II: Small-signal and conversion matrix sensitivity," *IEEE Trans. Electron Devices*, vol. 63, no. 3, pp. 1202–1208, 2016.

[73] A. Rogalski, P. Martyniuk, and M. Kopytko, "InAs/GaSb type-II superlattice infrared detectors: Future prospect," *Appl. Phys. Rev.*, vol. 4, no. 3, p. 031304, 2017.

[74] J. I. Mustafa, D. R. Rhiger, and C. W. Fulka, "Identifying and characterizing blinking pixels in photodiode arrays with hidden Markov models," in *Proc. SPIE 11503*, San Francisco, CA, Feb. 2020, p. 1150309.

[75] I.-H. Tan, G. L. Snider, L. D. Chang, and E. L. Hu, "A self-consistent solution of Schrödinger-Poisson equations using a nonuniform mesh," *J. Appl. Phys.*, vol. 68, no. 8, pp. 4071–4076, Oct. 1990.